

Deeply Self-Supervising Edge-to-Contour Neural Network Applied to Liver Segmentation

Minyoung Chung, Jingyu Lee, Minkyung Lee, Jeongjin Lee*, and Yeong-Gil Shin

Abstract—Accurate segmentation of liver is still challenging problem due to its large shape variability and unclear boundaries. The purpose of this paper is to propose a neural network based liver segmentation algorithm and evaluate its performance on abdominal CT images. First, we develop fully convolutional network (FCN) for volumetric image segmentation problem. To guide a neural network to accurately delineate target liver object, we apply self-supervising scheme with respect to edge and contour responses. Deeply supervising method is also applied to our low-level features for further combining discriminative features in the higher feature dimensions. We used 160 abdominal CT images for training and validation. Quantitative evaluation of our proposed network is presented with 8-fold cross validation. The result showed that our method successfully segmented liver more accurately than any other state-of-the-art methods without expanding or deepening the neural network. The proposed approach can be easily extended to other imaging protocols (e.g., MRI) or other target organ segmentation problems without any modifications of the framework.

Index Terms—CNN, deep learning, liver, neural network, segmentation.

I. INTRODUCTION

LIVER segmentation plays a crucial role for liver structural analysis, volume measures, and clinical operations (e.g., surgical planning). For clinical use, the accurate segmentation of liver is one of the key components of automated radiological diagnosis systems. Manual or semi-automatic segmentation of liver is a very impractical work due to its large shape variability and unclear boundaries. Unlike other organs, ambiguous boundaries with heart, stomach, pancreas, and fat make liver segmentation difficult. Thus, for computer-aided diagnosis (CAD) system, a fully automatic and accurate segmentation of liver will play an important role in medical imaging.

There are many proposed methods to segment liver in decades [1]–[10]. The most simple and intuitive approaches to perform liver segmentation are thresholding and region growing [1], [2]. Active contour model (ACM) approaches [3], [4] were also presented mainly using intensity distributions. However, such local intensity based approach easily

fails due to large variability of shapes and intensity contrasts. Shape prior based methods such as active shape model (ASM), statistical shape model (SSM), and registration based methods [5]–[7], [10]–[13] were presented to overcome such difficulties. Shape based methods were more successful than simple intensity based methods due to embedded shape priors. However, shape based methods also suffer from limited prior information because of the difficulty of embedding all inter patient organ shapes. That is, the number of training statistical model directly affects the model matching performance.

In recent years, deep neural network (DNN) gain popularity for many imaging applications [14]–[22]. For imaging applications, convolutional neural network (CNN) is the most effectively used network with respect to image classification [14]–[16], segmentation [17]–[20], [22], and enhancement [21], [23]. Active researches have been successfully applied CNN to medical image segmentation [22], [24]–[34]. U-net [24], applied contracting and expanding paths together with skip connections which successfully combined both low and high level features. U-net is not suitable for volumetric image segmentation because it is a fully convolutional network (FCN) based on 2D images. 2D based network architecture are not able to leverage complex 3D anatomical information. 3D U-net [25], tried to overcome the original U-net architecture to extract 3D contextual information via 3D convolutions with sparse annotation. However, 3D U-net had limitations of slice-based annotations. In [27], full 3D CNN based U-net like architecture is presented to segment volumetric medical images using dice coefficient loss metric to overcome class imbalance problem. Deep contour-aware network (DCAN) [28] tried to depict clear contours explicitly with multi-task framework. VoxResNet [26] is presented to perform brain tissue segmentation problem by voxelwise residual network. The authors used residual learning mechanism [15] to classify each voxel. Then, they used auto-context algorithm [35] to further refine voxelsize prediction results. Deeply supervised networks [36] is presented to hierarchically supervise multiple layers to segment medical images [31]. Deep supervision [31] allowed the network to be well-learned, fast-learned, and regularized. The authors also applied a fully connected conditional random field (CRF) model as a post-processing step to refine the segmentation results [31]. In [33], incorporation of global shape information with neural networks is presented. The authors tried to construct convolutional autoencoder networks to learn anatomical shape variations from training images [33].

In this paper, we propose a deeply self-supervising convolutional neural network with image edges. To guide a neural network to accurately delineate target liver object, we apply

Asterisk indicates corresponding author.

M. Chung is with the Department of Computer Science and Engineering, Seoul National University, Korea (e-mail: chungmy@cglab.snu.ac.kr).

J. Lee is with the Department of Computer Science and Engineering, Seoul National University, Korea (e-mail: leejingyu@cglab.snu.ac.kr).

M. Lee is with the Department of Computer Science and Engineering, Seoul National University, Korea (e-mail: mklee317@cglab.snu.ac.kr).

*J. Lee is with the Department of Computer Science and Engineering, Soong-sil University, Korea (e-mail: leejeongjin@ssu.ac.kr).

Y. Shin is with the Department of Computer Science and Engineering, Seoul National University, Korea (e-mail: yshin@snu.ac.kr).

self-supervising scheme with respect to edge and contour responses. Similar to [34], we designed our base network architecture as densely connected V-net [27] structure. We internally feed image gradient features and self-supervise contour responses to make it later combined more effectively in the high-level feature discriminators. Final layers delineate accurate liver shape and boundary by combining contour features and deeply supervised high-level features. A number of parameters and layers are effectively reduced via densely connected network architecture [37] while preserving network capability (i.e., accurate inference). Finally, we use learned DNN for automatic segmentation of liver from CT images.

The remainder of this paper is structured as follows. In section II, we will review several CNN models that are closely related to our method. Then, we describe our proposed method in section III. Experimental results, discussion, and conclusion are followed in section IV, V, and VI respectively.

II. RELATED WORK

In this section, we briefly review CNN mechanism and provide three major related works that contribute key steps of our method: V-net [27], deeply supervising networks [31], [36], and densely connected convolutional networks [37].

A. V-net

V-net [27] is a volumetric fully convolutional network for medical image segmentation. The authors extended the U-net architecture [24] to volumetric convolution (i.e., 3D convolution) and adopted U-net like downward and upward transitions (i.e., convolutional reduction and de-convolutional expanding of feature dimensions; see more details in the original paper: [27]) together with many skip connections by element-wise summation scheme. The authors also firstly presented dice loss to overcome class imbalance problem.

B. Deeply Supervising Network (DSN)

DSN is proposed to supervise a network to a deep level. That is, loss function penetrate through multiple layers in a deep neural network. Deeply supervising scheme makes intermediate features highly discriminative, so that the final classifier can easily make better discriminative classifier for the output. The another aspect of DSN is that training difficulty due to exploding and vanishing gradient problems can be alleviated by direct and deep gradient flows. In [31], 3D deep supervision mechanism is adopted to volumetric medical image segmentation. The authors exploited explicit supervision to hidden layers and those auxiliary losses were integrated to the final loss with the last output layer to back-propagate gradients.

C. Densely Connected Convolutional Network (DenseNet)

DenseNet [37] connects each layer to every other layer in a feed-forward fashion. The main advantage of the presented architecture is that gradient directly flows to deep layers accelerating learning procedure. Feature reusing also

TABLE I: TABLE OF NOTATIONS

Symbol	Definition	Expression
Ω	Image domain	$\Omega \in \mathbb{R}^3$
I	Input 3D image	normalized to [0..1]
$\ \nabla I\ $	Gradient response image	
Γ	Binary ground truth label	
Γ_d	Down-sampled Γ	by the factor of 2
Γ_c	Binary ground truth contour label	
C	Convolution	
C^-	De-convolution	Inverse convolution
s	Stride value of convolution	for each dimension
p	Zero-padding value	for each dimension
$B_{i,j}$	j^{th} DenseBlock-(k,n) at i^{th} level	Fig. 1
$F_{i,j}$	Output features of $B_{i,j}$	
D_i	Down transition layer for level i	$2^3 C, s = 2, p = 0$
U_i	Up transition layer for level i	$2^3 C^-, s = 2, p = 0$
T_c	Transformation for Γ_c	Fig. 2a
T_s^i	Transformation for Γ_d	Fig. 2a, $i \in 0, 1$
F_c	Output features of T_c	
F_s^i	Output features of T_s^i	
T_o^i	Out transition layer	Fig. 2b, $i \in 0, 1$
F_o^i	Output features of T_o^i	
W	Weights of the network	

strongly contribute to substantial reduction of the number of parameters. This structure can be viewed as implicit deep supervision network similar to explicit version [36]. The l^{th} layer gets the concatenation of all outputs of the preceding layers [37]:

$$x_l = H_l(x_0, x_1, \dots, x_{l-1}), \quad (1)$$

where x_l denotes the output of the l_{th} layer, $[x_0, x_1, \dots, x_{l-1}]$ refers to the concatenation of the feature-maps produced in the previous layers, and H_l denotes a non-linear transformation at l_{th} layer (e.g., composition of convolution, non-linear activation function). The feature reusing scheme of the DenseNet advantaging the reduction of parameters is an effective feature for 3D volumetric neural network because volume data easily lack of GPU memory for deep neural networks.

III. METHODOLOGY

Our model is composed of several layers: convolution, batch normalization [38], rectified linear unit (ReLU) non-linearity [39], densely connected layer block [37], and skip connections with both summation and concatenation scheme. Basic symbols for notations are presented in the Table I. The base unit component of our network is DenseBlock-(k,n) (Fig. 1). For deep supervision, two different transition layers are designed for contour, shape, and output transitions (Fig. 2). The detail of the architecture is shown in Fig. 3.

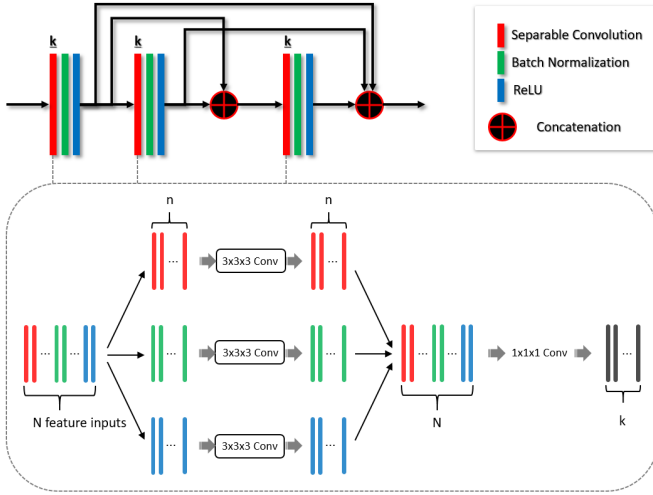


Fig. 1: Densely connected block component (i.e., DenseBlock-(k,n)). k indicates the number of features. The number of total features of a single DenseBlock-(k,n) becomes $3k$. Separable convolutions are applied to all DenseBlock-(k,n) units.

A. Network Architecture - Baseline

Let unit block, $B_{i,j}$, be the DenseBlock-(k,n) transformation at level i (i.e., down transitioned level starting with 0) and j^{th} block at level i . $B_{i,j}$ is composed of non-linear transformation series: convolution, batch normalization, and ReLU non-linear activation function (Fig. 1). These transformations are densely connected for feature reuse. Unlike in the original paper [37], we introduce depth-wise separable convolutions [40] in the densely connected block rather than bottleneck layers [41] or compression layers [37] for more efficient use of parameters. We write the output features of each $B_{i,j}$ layer as $F_{i,j}$. For down transition layers, D_i (i.e., down sampling feature dimensions; lower layers in Fig. 3), we get $F_{i,0}$ as input and down samples the feature map by the factor of 2 for each dimension by convolutions with stride 2. We preserve the number of feature of $F_{i,0}$. For up transition layers, U_i , we use de-convolution (i.e., transposed convolution) with restoring the number of features as the same as the skip connected upper layer for feature summation. Each up transitioned layers are summed with previous feature outputs (i.e., skip connection in Fig. 3) and pass through a DenseBlock-(k,n) unit (i.e., $B_{i,1}$, where $1 \leq i \leq 2$).

B. Network Architecture - Transition Layers

We applied two different deep supervision mechanism in our model: shape and contour (Fig. 2). Shape supervision is applied to $F_{1,1}$ with shape transition layers (i.e., T_s^i). Two identical transitions were applied separately for learning complementary residuals. Contour transition layers (i.e., T_c) are applied to low-level features for contour supervision. For contour transition, concatenation of $F_{0,0}$ and $\|\nabla I\|$ feature maps are fed to T_c for contour responses. Feature outputs of lower layers, $F_{2,1}$ and $F_{1,1}$, are up-scaled and concatenated with $F_{0,1}$ for further propagation of 0^{th} - level layers. After passing $B_{0,2}$, contour and shape responses (i.e., deeply

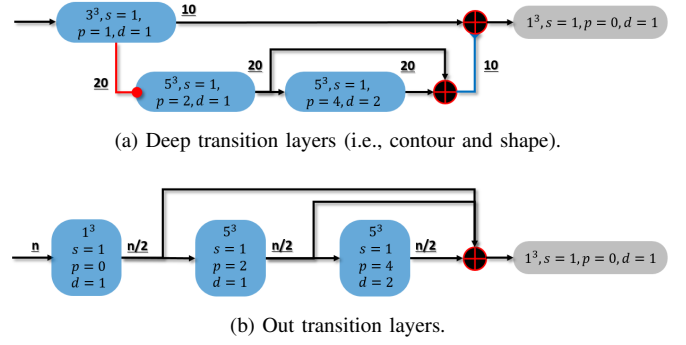


Fig. 2: Transition layers for (a) contour (T_c), shape (T_s^i), and (b) outs (T_o^i). Blue box indicates a series of convolution, batch normalization, and non-linear activation. Gray box indicates a single convolution layer. Each kernel size, stride, padding, and dilation value is specified.

supervised features) are sequentially concatenated for out-transition layers (Fig. 3). The final output is thus mixture of the predictions comprising contour, object shape, and deeply learned features.

For deep supervision of contour (i.e., F_c), we dynamically modified the ground-truth contour image, Γ_c , for every iteration:

$$\tilde{\Gamma}_c = \Gamma_c \otimes (\mathbf{y}_p), \quad (2)$$

where \otimes is an element-wise multiplication operator and \mathbf{y}_p is a binary image with respect to the threshold value, p :

$$\mathbf{y}_p(x) = \begin{cases} 1, & \text{if } \mathbf{y}(x) < p \\ 0, & \text{otherwise,} \end{cases} \quad (3)$$

where \mathbf{y} is the output probability prediction of our network for a given iteration. That is, we automatically erased the ground-truth contour labels (i.e., foreground voxels in Γ_c) if our network successfully delineated corresponding labels at the output. This modification procedure aid contour transition layers to effectively delineate misclassified contour region with respect to low-level features (e.g., edge). The output feature of contour transition is later combined with shape prediction for final liver object delineation.

C. Overall Loss Function

Let vectors of $\mathbf{x} = \{x_i \in R, i \in \Omega\}$ and $\mathbf{y} = \{y_i \in \{0,1\}, i \in \Omega\}$ for input image and ground-truth label respectively. The task of the given learning system is to model conditional probability distribution, $P(\mathbf{y}|\mathbf{x})$. To effectively model the probability distribution, we learn our network model to map the segmentation function $\phi(\mathbf{x}) : I(\mathbf{x}) \rightarrow \{0,1\}$ by minimizing the following loss function:

$$L_p(\mathbf{x}, \mathbf{y}; W) = \mathcal{D}(F_o^1, \Gamma) + \alpha \mathcal{D}(F_s^0 - F_s^1, \Gamma_d) + \beta \chi(F_c, \tilde{\Gamma}_c) + \gamma \|W\|_2^2, \quad (4)$$

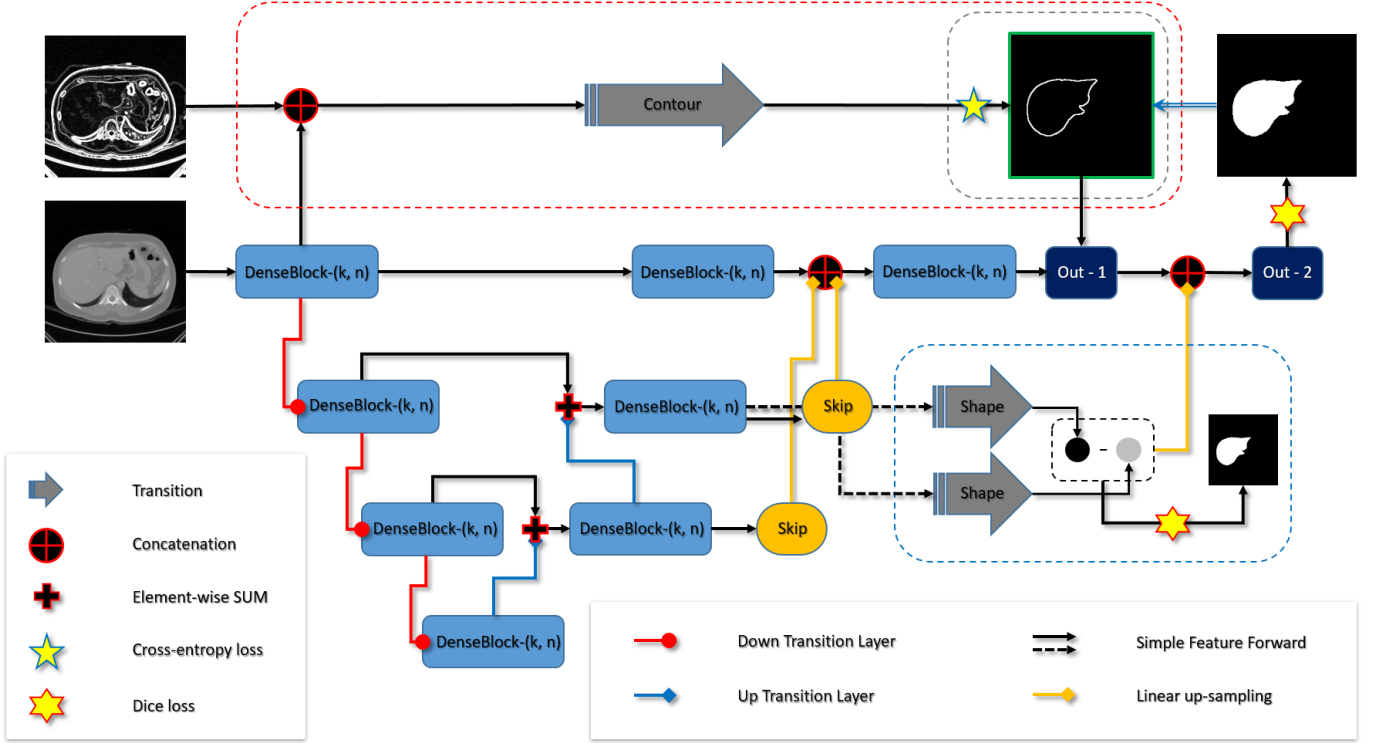


Fig. 3: Our proposed volumetric network architecture (best viewed in color). Red lines (i.e., circled arrows) and blue lines (i.e., squared arrows) indicate down and up transition layers (i.e., D_i and U_i) respectively. Orange lines (i.e., diamond arrows) indicate up sampling layers with linear interpolation scheme. Images are displayed as 2D for simplicity.

where \mathcal{D} indicates dice loss [27], χ indicates softmax-cross-entropy loss,

$$\chi(\mathbf{x}, \mathbf{y}) = \sum_i (-w_i \log(\frac{\exp(\mathbf{x}[y_i])}{\sum_j \exp(\mathbf{x}[j])})). \quad (5)$$

α, β , and γ in (4) are weighting parameters. w_i in (5) is class balancing weights. The output of the network is made by applying softmax to the final output feature maps.

D. Data Preparation and Augmentation

We acquired 160 subjects in total: 90 subjects from publicly available dataset¹ by the authors in [34], 20 subjects from MICCAI-Sliver07 dataset [8], 20 subjects from 3Dircadb², and additional 30 annotated subjects with the help of clinical experts in the field. In the dataset, a slice thickness ranged from 0.5mm to 5.0mm and pixel sizes ranged from 0.6mm to 1.0mm.

For the training dataset, we have resampled all abdominal CT images by 128x128x64. We pre-processed the image using fixed windowing values: level=10 and width=700 (i.e., clipped the intensity values under -340 and over 360). After re-scaling, we have normalized the input images into the range of [0..1] value for each voxel. On the fly random affine deformations are then applied to the dataset for each iteration with 80%

probability. We finally perform cutout image augmentation [42] with 80% probability. We did not constrain the position of cutout mask with respect to boundaries. We applied random sized zero mask with the range of $L/5 \leq l \leq L/4$ where l and L are length of mask and length of image for each dimension, respectively. To the best of our knowledge, this is the first work to apply cutout [42] augmentation to image segmentation problem. We presented the effect of the cutout augmentations in the experiment section IV.

E. Learning the Network

For initializing network weights, 'Xavier' initialization [43] is used for all the weights of the proposed network. During training the network, we have fixed the loss parameters as $\alpha = 1$, $\beta = 1$, and $\gamma = 0.1$ in (4). We have set the parameter p as 1 until 100 epochs, and decayed by multiplying 0.9 for every 10 epoch until 0.5 (i.e., the minimum value of p). For dense block unit, we used DenseBlock-(16,4) (i.e., $k = 16, n = 4$). We have used Adam optimizer with batch size 4 and learning rate 0.001. We decayed the learning rate by multiplying 0.1 for every 50 epoch. We trained the network for 300 epochs using Intel i7-7700K desktop system with 4.2 GHz processor, 32 GB of memory, and Nvidia Titan Xp GPU machine. It took 10 hours for all training procedures.

IV. EXPERIMENTS AND RESULTS

In our experiments, we evaluate learning curves and results of the proposed network comparing with other FCN

¹DOI:<http://doi.org/10.5281/zenodo.1169361>

²<https://www.ircad.fr/research/3dircadb>

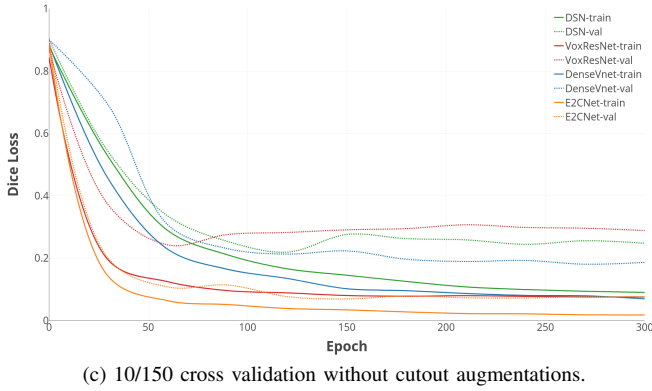
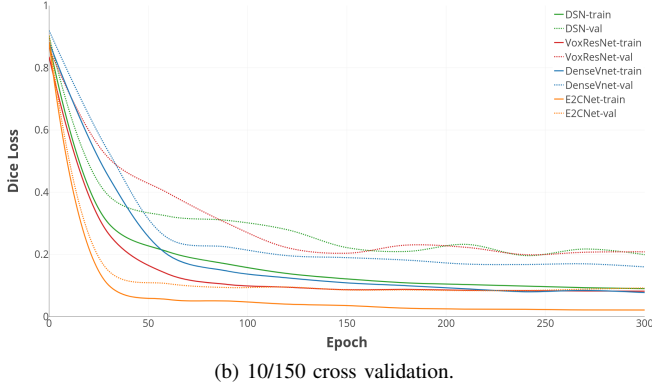
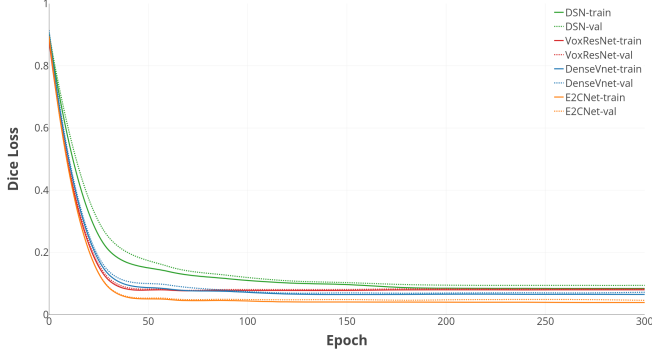


Fig. 4: Learning curves of DSN [31], VoxResNet [26], DenseVNet [34], and E2CNet with multiple cross validations: (a) used 140 images for training and 20 images for validation (i.e., 8-fold cross validation). (b) and (c) used 10 images for training and 150 images for validation. (c) shows the learning curve without cutout [42] augmentation.

based models. We experimented DSN [31], VoxResNet [26], DenseVNet [34], and our proposed network, E2CNet for performance evaluation.

A. Learning Curve

In Fig. 4, learning curve with dice loss is plotted. All hyper parameters (e.g., learning rate, optimizer) were set as specified in the original papers. We first designed 8-fold cross validation for performance evaluation (i.e., 140 training images

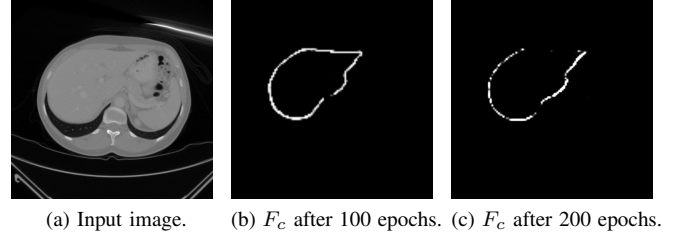


Fig. 5: Visualization of contour feature maps (i.e., F_c) after training (b) 100 and (c) 200 epochs.

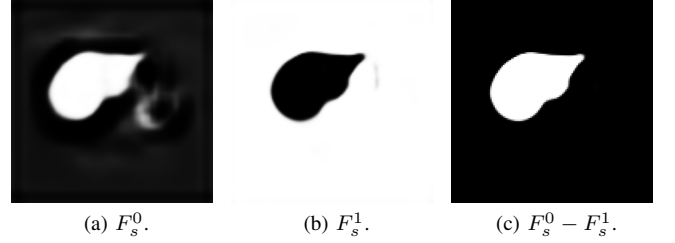


Fig. 6: Visualization of shape feature maps (i.e., F_s^i) after full training. (c) shows the subtraction result of F_s^i features.

and 20 validation images). Plot in Fig. 4a indicates that our proposed network achieved the most successful training result. Other networks suffered from learning all training images successfully. The quantitative results are presented in Table II and III. We have additionally designed special experimental setting with 10 training images and 150 validation images (Fig. 4b and 4c). We believe that this experimental setting approximately proxies the real life deep learning problem and shows the extremely generalized regularization analysis. Overall validation errors increased in the special cross validation with 10 training images (Fig. 4b). Meanwhile, our proposed network did not over-fit (i.e., lowest generalization error) to training images compared to other networks. Fig. 4c shows the worse generalization curve without cutout augmentation [42] indicating that cutout augmentation greatly aids the network training to be generalized. In all training experiments, our proposed network made fastest convergence, showed the lowest loss value, and resulted in best generalization.

B. Edge-to-Contour and Shape Feature Layers

We have visualized the output feature map of T_c (i.e., F_c) in Fig. 5. For 100 epochs, contour transition layers were supervised to delineate entire ground-truth contour. Parameter p decays after 100 epoch so that dynamically modified contour (i.e., (2)) is supervised for supplementary contour delineation.

The effects of residuals in shape transition layers are showed in Fig. 6. Both T_s^0 and T_s^1 learns complementary features (Fig. 6a and Fig. 6b) for accurate shape delineation by subtraction scheme.

C. Quantitative Evaluations

We have evaluated segmentation results by dice similarity coefficient (DSC), 95% Hausdorff distance (HD), and average

TABLE II
QUANTITATIVE EVALUATION OF 8-FOLD CROSS VALIDATION WITH MEDIAN METRIC.

Methods	DSC	HD [mm]	ASD [mm]	Sensitivity	Precision
DSN	0.94	5.60	1.60	0.95	0.94
VoxResNet	0.93	6.71	1.78	0.92	0.96
DenseVNet	0.92	10.13	2.27	0.97	0.88
E2CNet	0.96	3.99	1.20	0.97	0.97
E2CNet-C	0.96	4.56	1.21	0.97	0.96
E2CNet-S	0.96	4.21	1.19	0.96	0.97
E2CNet-R	0.96	5.25	1.27	0.96	0.96

TABLE III
MEAN AND STANDARD DEVIATION OF 8-FOLD CROSS VALIDATION.

Metric	DSN	VoxResNet	DenseVNet	E2CNet
DSC	0.94 ± 0.02	0.93 ± 0.02	0.92 ± 0.02	0.96 ± 0.01
HD	7.49 ± 4.21	7.99 ± 4.04	11.47 ± 6.60	5.25 ± 2.70
ASD	1.77 ± 0.51	1.93 ± 0.48	2.53 ± 0.59	1.17 ± 0.30
S	0.93 ± 0.04	0.91 ± 0.04	0.97 ± 0.02	0.96 ± 0.03
P	0.94 ± 0.02	0.95 ± 0.02	0.88 ± 0.03	0.96 ± 0.02

symmetric distance (ASD), sensitivity (S), and precision (P). Dice similarity coefficient is defined by

$$DSC(X, Y) = \frac{2|X \cap Y|}{|X| + |Y|}, \quad (6)$$

where $|\cdot|$ is a cardinality of a set. Letting \mathbf{S}_X as a set of surface voxels of a set X , the shortest distance of an arbitrary voxel p is defined as [8]:

$$d(p, \mathbf{S}_X) = \min_{s_X \in \mathbf{S}_X} \|p - s_X\|_2. \quad (7)$$

Hausdorff distance (HD) is then given by [8]:

$$HD(X, Y) = \max\left\{\max_{s_X \in \mathbf{S}_X} d(s_X, \mathbf{S}_Y) + \max_{s_Y \in \mathbf{S}_Y} d(s_Y, \mathbf{S}_X)\right\}. \quad (8)$$

Defining the distance function

$$D(\mathbf{S}_X, \mathbf{S}_Y) = \sum_{s_X \in \mathbf{S}_X} d(s_X, \mathbf{S}_Y), \quad (9)$$

the average symmetric surface distance (ASD) can be defined as [8]:

$$ASD(X, Y) = \frac{1}{|\mathbf{S}_X| + |\mathbf{S}_Y|} (D(\mathbf{S}_X, \mathbf{S}_Y) + D(\mathbf{S}_Y, \mathbf{S}_X)). \quad (10)$$

Sensitivity and precision are defined as follows:

$$S = \frac{TP}{TP + FN}, \quad (11)$$

$$P = \frac{TP}{TP + FP} \quad (12)$$

where TP , FN , and FP are the number of true positive, false negative, and false positive voxel, respectively. In (8), 95% of voxels were calculated in (7) in order to exclude 5% outlying

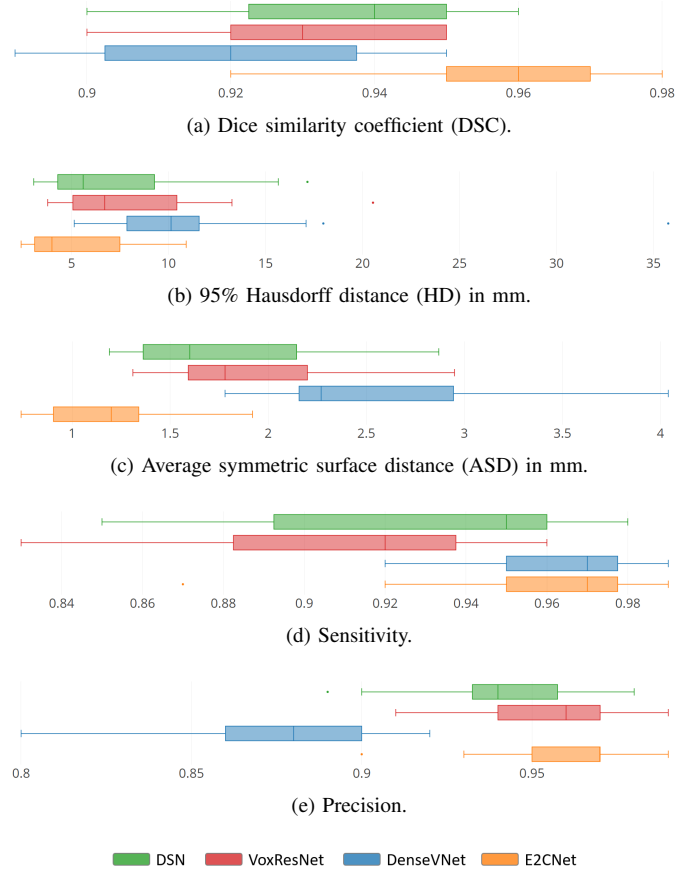


Fig. 7: Box plots of segmentation metrics for 8-fold performance evaluations.

voxels. This is for generalized evaluation of distance without portal vein variations (Fig. 8). 8-fold cross validation is used for quantitative results in Table II and III. Visual box plot of Table III is presented in Fig. 7. Our proposed E2CNet showed the best segmentation results within all evaluations. Especially, DenseVNet failed to segment liver accurately mainly by two significant reasons: 1) the network use too low resolution and 2) shape prior has weak representative power. That is, with too coarse dimensions of image, segmentation result suffers from accurate delineation of object in the original domain. Furthermore, 12^3 resolution of shape prior is way too small

and training images must be accurately and manually cropped to make full use of learned shape prior. There is no specific metric presented in the original paper [34] to crop testing images automatically.

We have extended our experiments with our network variants: E2CNet without contour transition layer (i.e., removing red box in Fig. 3; E2CNet-C), without shape transition layer (i.e., removing blue box in Fig. 3; E2CNet-S), and without residual shape estimation layer (i.e., removing black box in Fig. 3; E2CNet-R). In case of E2CNet-R, only one shape transition layer (i.e., T_s^0) is used for single shape feature estimation. The accuracy of our network variants slightly decreased compared to the proposed E2CNet. DSC, sensitivity and precision scores of the variants were preserved while distance errors (i.e., 95% HD, ASD) slightly increased. E2CNet-S showed the lowest distance errors among the variants while E2CNet-R showed the highest. This indicates that residual shape estimation process is critical for using accurate shape estimation pass. When using E2CNet-R network, the F_s^0 feature was similar to Fig. 6a which lead to the inaccurate output result. Without residuals, we might have to design a more complex and deep transition layers for shape estimation which might lead to over-fitting. The result of E2CNet-C indicates that contour transition part plays a key role for accurate delineation of an object.

The visual result of an example liver subject is presented in Fig. 8. As it is clearly visualized, our proposed E2CNet successfully segmented liver with proper guidelines of contour and accurate shape estimation. All networks including ours suffered to segment portal vein entry region accurately. However, we found out that our training database (i.e., clinically annotated ground-truth images) had serious internal variation in portal vein entry region. Some clinicians included the vessels while some excluded the major entry vessel region. We suggest concurrent and integrated liver and vascular system segmentation framework to be built in the future so that the variability of annotations can be overcome. In case of DenseVNet, inaccurate shape prior seriously affected the final output Fig. 8d.

V. DISCUSSION

Segmentation of organs in medical imaging is still a very challenging problem. Edge feature is unquestionably the most important feature for object delineation. However, edge feature is hard to be identified in many cases (e.g., unclear boundaries, false edges in contrast enhanced vessels). That is, object segmentation problem cannot be solved accurately without any additional higher-level information. In recent years, the most promising methods to accurately segment medical objects are using shape priors or neural networks. Our proposed network avoided to use shape priors but rather guided the neural network to estimate liver shape. We have used two major neural network branches: contour estimation and shape estimation. This network might be seen as similar to multi-task learning framework. However, we do not enforce the network to explicitly inference multiple tasks. Our network internally guide weights to make object contour features via edge responses

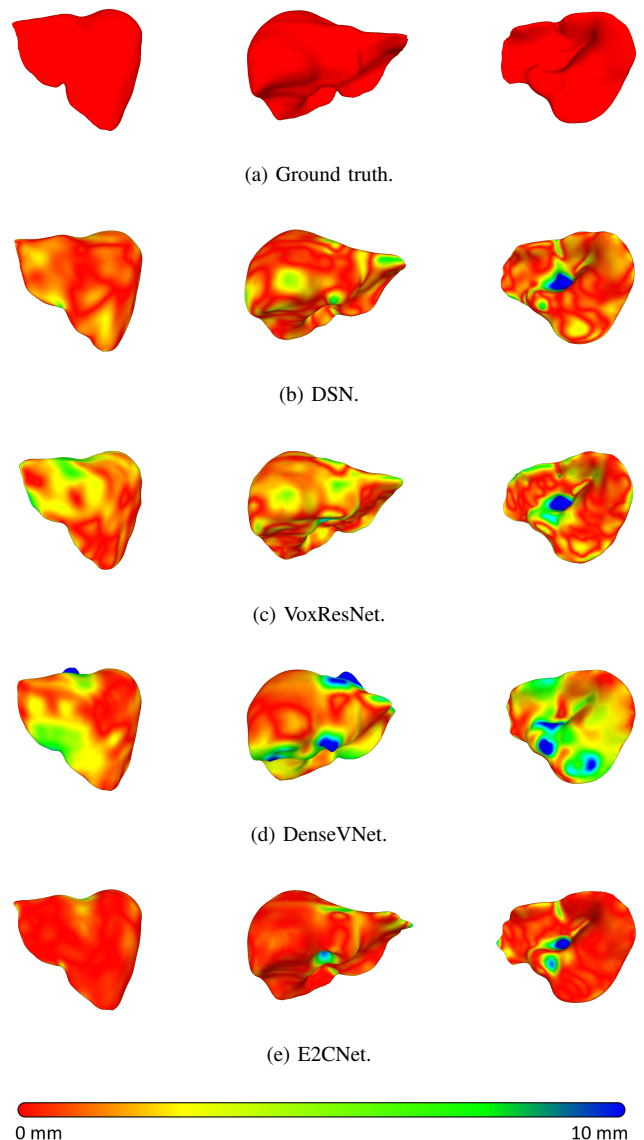


Fig. 8: Visualizations of 8-fold segmentation results. Surface color is visualized with respect to distance to ground-truth surface. Every metric failed to accurately segment portal vein entry region due to the large variance of annotated training images.

(i.e., gradient magnitude of an image) without supervising the entire contour image. We supervised the network with modified contour image. The main underlying principle of the proposed network is to make contour delineation pass concentrate on the missing contour part of an object (i.e., fine details of an object that are easily to be misclassified by the end-to-end learning). There are two important reasons for the proposed method: 1) Even with powerful deep neural network, unclear boundaries are very challenging to be discriminated as a contour. 2) Contour regions in unclear boundaries can be well delineated by global shapes. Finally, we have merged three strong discriminative features (i.e., shape, contour details, and deep features) for the best segmentation results. The proposed network can be intuitively interpreted as a strong edge to

contour guided shape estimation.

Our proposed network can be easily extended to other imaging protocols (e.g., MRI) or other target organ segmentation problems without any network modifications. For effective modification of our proposed network to other applications, we recommend to modify parameters of dense block (Fig. 1) and p (i.e., threshold value to determine the misclassified voxels). k and n parameters in dense block adjust the complexity of a network and p adjusts the work load of contour transition (i.e., T_c). Higher value of p , more contour region will be required to be delineated in the contour estimation pass. In our experiments (i.e., liver segmentation), the parameter p was not sensitive to the presented results.

VI. CONCLUSION

In this work, we have designed a fully convolutional neural network for image segmentation. Our proposed network combine shape and contour features to accurately delineate target object. We divided the network into big two branches for shape estimation and supplementary contour estimation. Two branches act as a complement for each other. Densely connected block with separable convolution is used as a building block of our network. Dense connections and separable convolutions made the network more compact and representative that our proposed network successfully performed liver segmentation problem without deepening or widening the neural network. Much fewer parameters compared to other models resulted in good regularization effect.

REFERENCES

- [1] S.-J. Lim, Y.-Y. Jeong, and Y.-S. Ho, "Automatic liver segmentation for volume measurement in ct images," *Journal of Visual Communication and Image Representation*, vol. 17, no. 4, pp. 860–875, 2006.
- [2] L. Rusko, G. Bekes, G. Nemeth, and M. Fidrich, "Fully automatic liver segmentation for contrast-enhanced ct images," *MICCAI Wshp. 3D Segmentation in the Clinic: A Grand Challenge*, vol. 2, no. 7, 2007.
- [3] K. Suzuki, R. Kohlbrenner, M. L. Epstein, A. M. Obajuluwa, J. Xu, and M. Hori, "Computer-aided measurement of liver volumes in ct by means of geodesic active contour segmentation coupled with level-set algorithms," *Medical physics*, vol. 37, no. 5, pp. 2159–2166, 2010.
- [4] J. Lee, N. Kim, H. Lee, J. B. Seo, H. J. Won, Y. M. Shin, Y. G. Shin, and S.-H. Kim, "Efficient liver segmentation using a level-set method with optimal detection of the initial liver boundary from level-set speed images," *Computer Methods and Programs in Biomedicine*, vol. 88, no. 1, pp. 26–38, 2007.
- [5] X. Zhang, J. Tian, K. Deng, Y. Wu, and X. Li, "Automatic liver segmentation using a statistical shape model with optimal surface detection," *IEEE Transactions on Biomedical Engineering*, vol. 57, no. 10, pp. 2622–2626, 2010.
- [6] T. Okada, R. Shimada, Y. Sato, M. Hori, K. Yokota, M. Nakamoto, Y.-W. Chen, H. Nakamura, and S. Tamura, "Automated segmentation of the liver from 3d ct images using probabilistic atlas and multi-level statistical shape model," in *International Conference on Medical Image Computing and Computer-Assisted Intervention*. Springer, 2007, pp. 86–93.
- [7] H. Ling, S. K. Zhou, Y. Zheng, B. Georgescu, M. Suehling, and D. Comaniciu, "Hierarchical, learning-based automatic liver segmentation," in *Computer Vision and Pattern Recognition, 2008. CVPR 2008. IEEE Conference on*. IEEE, 2008, pp. 1–8.
- [8] T. Heimann, B. Van Ginneken, M. A. Styner, Y. Arzhaeva, V. Aurich, C. Bauer, A. Beck, C. Becker, R. Beichel, G. Bekes *et al.*, "Comparison and evaluation of methods for liver segmentation from ct datasets," *IEEE transactions on medical imaging*, vol. 28, no. 8, pp. 1251–1265, 2009.
- [9] P. Campadelli, E. Casiraghi, and A. Esposito, "Liver segmentation from computed tomography scans: A survey and a new algorithm," *Artificial intelligence in medicine*, vol. 45, no. 2-3, pp. 185–196, 2009.
- [10] E. van Rikxoort, Y. Arzhaeva, and B. van Ginneken, "Automatic segmentation of the liver in computed tomography scans with voxel classification and atlas matching," in *Proceedings of the MICCAI Workshop*, vol. 3. Citeseer, 2007, pp. 101–108.
- [11] T. Heimann, H. Meinzer, and I. Wolf, "A statistical deformable model for the segmentation of liver ct volumes using extended training data," *Proc. MICCAI Work*, pp. 161–166, 2007.
- [12] D. Kainmüller, T. Lange, and H. Lamecker, "Shape constrained automatic segmentation of the liver based on a heuristic intensity model," in *Proc. MICCAI Workshop 3D Segmentation in the Clinic: A Grand Challenge*, 2007, pp. 109–116.
- [13] A. Wimmer, G. Soza, and J. Hornegger, "A generic probabilistic active shape model for organ segmentation," in *International Conference on Medical Image Computing and Computer-Assisted Intervention*. Springer, 2009, pp. 26–33.
- [14] K. Simonyan and A. Zisserman, "Very deep convolutional networks for large-scale image recognition," *arXiv preprint arXiv:1409.1556*, 2014.
- [15] K. He, X. Zhang, S. Ren, and J. Sun, "Deep residual learning for image recognition," in *Proceedings of the IEEE conference on computer vision and pattern recognition*, 2016, pp. 770–778.
- [16] C. Szegedy, S. Ioffe, V. Vanhoucke, and A. A. Alemi, "Inception-v4, inception-resnet and the impact of residual connections on learning," in *AAAI*, vol. 4, 2017, p. 12.
- [17] J. Long, E. Shelhamer, and T. Darrell, "Fully convolutional networks for semantic segmentation," in *Proceedings of the IEEE conference on computer vision and pattern recognition*, 2015, pp. 3431–3440.
- [18] H. Noh, S. Hong, and B. Han, "Learning deconvolution network for semantic segmentation," in *Proceedings of the IEEE International Conference on Computer Vision*, 2015, pp. 1520–1528.
- [19] V. Badrinarayanan, A. Kendall, and R. Cipolla, "Segnet: A deep convolutional encoder-decoder architecture for image segmentation," *IEEE transactions on pattern analysis and machine intelligence*, vol. 39, no. 12, pp. 2481–2495, 2017.
- [20] J. Fu, J. Liu, Y. Wang, and H. Lu, "Stacked deconvolutional network for semantic segmentation," *arXiv preprint arXiv:1708.04943*, 2017.
- [21] C. Dong, C. C. Loy, K. He, and X. Tang, "Image super-resolution using deep convolutional networks," *IEEE transactions on pattern analysis and machine intelligence*, vol. 38, no. 2, pp. 295–307, 2016.
- [22] S. Jégou, M. Drozdal, D. Vazquez, A. Romero, and Y. Bengio, "The one hundred layers tiramisu: Fully convolutional densenets for semantic segmentation," in *Computer Vision and Pattern Recognition Workshops (CVPRW)*, 2017 *IEEE Conference on*. IEEE, 2017, pp. 1175–1183.
- [23] H. C. Burger, C. J. Schuler, and S. Harmeling, "Image denoising: Can plain neural networks compete with bm3d?" in *Computer Vision and Pattern Recognition (CVPR)*, 2012 *IEEE Conference on*. IEEE, 2012, pp. 2392–2399.
- [24] O. Ronneberger, P. Fischer, and T. Brox, "U-net: Convolutional networks for biomedical image segmentation," in *International Conference on Medical image computing and computer-assisted intervention*. Springer, 2015, pp. 234–241.
- [25] Ö. Çiçek, A. Abdulkadir, S. S. Lienkamp, T. Brox, and O. Ronneberger, "3d u-net: learning dense volumetric segmentation from sparse annotation," in *International Conference on Medical Image Computing and Computer-Assisted Intervention*. Springer, 2016, pp. 424–432.
- [26] H. Chen, Q. Dou, L. Yu, J. Qin, and P.-A. Heng, "Voxresnet: Deep voxelwise residual networks for brain segmentation from 3d mr images," *NeuroImage*, 2017.
- [27] F. Milletari, N. Navab, and S.-A. Ahmadi, "V-net: Fully convolutional neural networks for volumetric medical image segmentation," in *3D Vision (3DV)*, 2016 *Fourth International Conference on*. IEEE, 2016, pp. 565–571.
- [28] H. Chen, X. Qi, L. Yu, Q. Dou, J. Qin, and P.-A. Heng, "Dcan: Deep contour-aware networks for object instance segmentation from histology images," *Medical image analysis*, vol. 36, pp. 135–146, 2017.
- [29] K. Kamnitsas, C. Ledig, V. F. Newcombe, J. P. Simpson, A. D. Kane, D. K. Menon, D. Rueckert, and B. Glocker, "Efficient multi-scale 3d cnn with fully connected crf for accurate brain lesion segmentation," *Medical image analysis*, vol. 36, pp. 61–78, 2017.
- [30] M. Havaei, A. Davy, D. Warde-Farley, A. Biard, A. Courville, Y. Bengio, C. Pal, P.-M. Jodoin, and H. Larochelle, "Brain tumor segmentation with deep neural networks," *Medical image analysis*, vol. 35, pp. 18–31, 2017.
- [31] Q. Dou, L. Yu, H. Chen, Y. Jin, X. Yang, J. Qin, and P.-A. Heng, "3d deeply supervised network for automated segmentation of volumetric medical images," *Medical image analysis*, vol. 41, pp. 40–54, 2017.
- [32] L.-C. Chen, G. Papandreou, I. Kokkinos, K. Murphy, and A. L. Yuille, "DeepLab: Semantic image segmentation with deep convolutional nets, atrous convolution, and fully connected crfs," *IEEE transactions on*

- pattern analysis and machine intelligence*, vol. 40, no. 4, pp. 834–848, 2018.
- [33] O. Oktay, E. Ferrante, K. Kamnitsas, M. Heinrich, W. Bai, J. Caballero, S. A. Cook, A. de Marvao, T. Dawes, D. P. O'Regan *et al.*, “Anatomically constrained neural networks (acnns): application to cardiac image enhancement and segmentation,” *IEEE transactions on medical imaging*, vol. 37, no. 2, pp. 384–395, 2018.
 - [34] E. Gibson, F. Giganti, Y. Hu, E. Bonmati, S. Bandula, K. Gurusamy, B. Davidson, S. P. Pereira, M. J. Clarkson, and D. C. Barratt, “Automatic multi-organ segmentation on abdominal ct with dense v-networks,” *IEEE Transactions on Medical Imaging*, 2018.
 - [35] Z. Tu and X. Bai, “Auto-context and its application to high-level vision tasks and 3d brain image segmentation,” *IEEE Transactions on Pattern Analysis and Machine Intelligence*, vol. 32, no. 10, pp. 1744–1757, 2010.
 - [36] C.-Y. Lee, S. Xie, P. Gallagher, Z. Zhang, and Z. Tu, “Deeply-supervised nets,” in *Artificial Intelligence and Statistics*, 2015, pp. 562–570.
 - [37] G. Huang, Z. Liu, K. Q. Weinberger, and L. van der Maaten, “Densely connected convolutional networks,” in *Proceedings of the IEEE conference on computer vision and pattern recognition*, vol. 1, no. 2, 2017, p. 3.
 - [38] S. Ioffe and C. Szegedy, “Batch normalization: Accelerating deep network training by reducing internal covariate shift,” *arXiv preprint arXiv:1502.03167*, 2015.
 - [39] V. Nair and G. E. Hinton, “Rectified linear units improve restricted boltzmann machines,” in *Proceedings of the 27th international conference on machine learning (ICML-10)*, 2010, pp. 807–814.
 - [40] F. Chollet, “Xception: Deep learning with depthwise separable convolutions,” *arXiv preprint*, pp. 1610–02357, 2017.
 - [41] C. Szegedy, V. Vanhoucke, S. Ioffe, J. Shlens, and Z. Wojna, “Rethinking the inception architecture for computer vision,” in *Proceedings of the IEEE conference on computer vision and pattern recognition*, 2016, pp. 2818–2826.
 - [42] T. DeVries and G. W. Taylor, “Improved regularization of convolutional neural networks with cutout,” *arXiv preprint arXiv:1708.04552*, 2017.
 - [43] X. Glorot and Y. Bengio, “Understanding the difficulty of training deep feedforward neural networks,” in *Proceedings of the thirteenth international conference on artificial intelligence and statistics*, 2010, pp. 249–256.